Global and Planetary Change 252 (2025) 104868

Contents lists available at ScienceDirect

Global and Planetary Change

journal homepage: www.elsevier.com/locate/gloplacha

Research Article

Stability up until the end: Disruption, recovery and the latest Permian nitrogen cycle at Penglaitan, China

Shane D. Schoepfer [a,*], Eldridge Machen II [a], Hannah Cothren [b], Lei Xiang [c], Hua Zhang [c,*]

[a] Department of Geosciences and Natural Resources, Western Carolina University, Cullowhee, NC, USA
[b] Department of Earth and Space Sciences, University of Washington, Seattle, WA, USA
[c] State Key Laboratory of Palaeobiology and Stratigraphy, Nanjing Institute of Geology and Palaeontology, Chinese Academy of Sciences (CAS), Nanjing 210008, China

ARTICLE INFO

Editor: Dr. Maoyan Zhu

Keywords:
Changhsingian
Denitrification
Oligotrophic
Extinction
Volcanism

ABSTRACT

Negative organic sedimentary nitrogen isotope excursions are a common feature of sedimentary records spanning the end-Permian mass extinction (EPME). These excursions likely reflect global-scale perturbations of the marine nitrogen cycle. However, most EPME sections offer too little stratigraphic resolution to assess the timing, nature, and local ecological impacts of these disruptions. The Penglaitan Northern Bank section in Guangxi, China, offers an opportunity to explore the end-Permian nitrogen cycle in over 600 m of Changhsingian strata deposited in marginal marine environments of the Nanpanjiang Basin. The succession contains numerous volcanogenic sandstones and crystalline tuffs, defining a pattern of disruption and recovery on ecological timescales that can be compared to the more impactful biogeochemical changes associated with the EPME.

Organic carbon and nitrogen isotopes in the Penglaitan Northern Bank section are stable throughout the majority of the Changhsingian, with nitrogen isotope values consistent with a background 'greenhouse' climate nitrogen cycle. This stability in the nitrogen cycle is interrupted by the latest Permian transgression, beginning at 252.0 Ma. During the transgression, nitrogen isotope values become considerably more variable, ranging from negative values indicative of N fixation in an oligotrophic environment to more enriched values reflecting the incursion of anoxic, denitrifying waters. Nitrogen isotope values in the earliest Triassic stabilize, but remain lower than the Changhsingian baseline. The negative $\delta^{15}N$ excursions seen in other sections globally likely represent condensed expressions of the more complex nitrogen cycle processes revealed at Penglaitan.

At Penglaitan, $\delta^{15}N$ instability precedes the paleontologically defined extinction at the EPME and demonstrates that changes to marine biogeochemical cycles were diachronous with respect to local species extinctions, which may have been proximally driven by local volcanism and facies changes. While unstable nutrient cycles may have stressed marine ecosystems in the latest Changhsingian, they did not immediately push these communities beyond their ability to recover from episodic disturbance by volcanism.

1. Introduction

The end-Permian mass extinction (EPME) was the most devastating biodiversity crisis of the Phanerozoic, corresponding with an estimated loss of approximately 90 % of marine species and 86 % of terrestrial species (Erwin et al., 2002; Benton and Twitchett, 2003). The extinction is linked to a series of cascading environmental changes ultimately rooted in the emplacement of the Siberian Traps Large Igneous Province (Burgess and Bowring, 2015; Bond and Grasby, 2017; Algeo and Shen, 2024), including rapid and intense climatic warming (Joachimski et al., 2012; Sun et al., 2012; Romano et al., 2013), ocean stratification (Kidder and Worsley, 2010; Song et al., 2012) leading to widespread marine anoxia and euxinia (Isozaki, 1997; Wignall and Twitchett, 2002; Grice et al., 2005; Hays et al., 2007; Song et al., 2014; Lau et al., 2016; Zhang et al., 2018a; Grasby et al., 2021), ocean acidification (Payne et al., 2007, 2010), the devastation of terrestrial ecosystems (Benton and Newell, 2014; Aftabuzzaman et al., 2021) and, rapid sedimentation in marginal marine ecosystems (Algeo and Twitchett, 2010; Algeo et al., 2011).

Records of the effects of the EPME are spatially complex, manifesting differently across the diverse ecosystems of the Late Permian world (Penn et al., 2018; Dal Corso et al., 2022). The marine extinction may

* Corresponding authors.
E-mail addresses: sschoepfer@email.wcu.edu (S.D. Schoepfer), hzhang@nigpas.ac.cn (H. Zhang).

https://doi.org/10.1016/j.gloplacha.2025.104868
Received 20 November 2024; Received in revised form 24 March 2025; Accepted 28 April 2025
Available online 29 April 2025

have been diachronous on the order of up to 100 kyr (Algeo et al., 2012), and Permian 'holdovers' are abundant in some earliest Triassic taxa (Foster et al., 2018) indicating that some Permian populations persisted through the extinction interval. While the global scale 'kill mechanisms' listed above been invoked to explain the disappearance of species and higher-order taxa, the flora and fauna living during the end of the Paleozoic Era were most likely subject to mortality as a result of proximal, ecological drivers, including predation, food scarcity, and the physical destruction of ecosystem substrate (e.g., Godbold et al., 2017), operating on timescales relevant to the lifespans of individual organisms. These ecological factors interacted with the shrinking of ecospace driven by global-scale environmental changes (Song et al., 2014), resulting in reproductive failure and eventual populations collapse and extinction (Pietsch et al., 2019; Cribb et al., 2023).

Disruptions to the nitrogen cycle are among the most consistent aspects of the EPME across a range of marine environments, suggesting changes in nutrients occurred on a global scale (Luo et al., 2011; Schoepfer et al., 2012; Knies et al., 2013; Algeo et al., 2014; Grasby et al., 2016, 2020; Zakharov et al., 2021; Schoepfer and Henderson, 2021; Du et al., 2023). A negative excursion in the $\delta^{15}N$ of sedimentary organic nitrogen is essentially ubiquitous across all published EPME sections (Algeo et al., 2014), reflecting an increased contribution of direct N fixation by cyanobacteria in response to nitrogen limitation (Stüeken et al., 2024). The larger magnitude of this excursion along the subtropical margin of the Pangaean supercontinent likely records the weakening of western-boundary upwelling (Schoepfer et al., 2012, 2013; Knies et al., 2013; Schoepfer and Henderson, 2021), while the small excursion seen in Japanese pelagic sections may be because these distal environments were already dependent on N fixation prior to the EPME crisis (Schoepfer, 2014).

Nitrogen limitation in marine environments may have resulted from enhanced denitrification in anoxic water masses. While this may have led to ammonium becoming the predominant form of dissolved nitrogen in anoxic water masses (Sun et al., 2019; Du et al., 2023), it is also possible that the decreased residence time of marine nitrate led to lower standing nitrate inventories and enhanced compensatory nitrogen fixation without a full transition to an ammonium ocean (Kidder and Worsley, 2010; Stüeken et al., 2024). At the same time that fixed nitrogen was becoming less available, terrigenous nutrients such as iron and phosphorus likely became more abundant (Schobben et al., 2015), and changes in primary productivity across the EPME were spatially complex (Algeo et al., 2013; Shen et al., 2015). Declining primary productivity, resulting from decreased overall nutrient availability, may have contributed to the extinction in a variety of marginal marine settings (Grasby et al., 2016, 2020). This pattern is especially pronounced on the South China Block (Algeo et al., 2013; Shen et al., 2015; Zhang et al., 2018b), where oceans remained highly stratified (Song et al., 2012) and oligotrophic well into the Early Triassic (Du et al., 2023).

While the EPME has been extensively studied in sections across the globe, many of these sections are stratigraphically condensed or contain substantial unconformities, limiting their utility as records of extinction on ecological timescales. In the Meishan D section, the Global Stratotype Section and Point (GSSP) that defines the Permian-Triassic Boundary, the EPME is recorded within a ~ 0.3 m interval (Jin et al., 2000; Yin et al., 2007). Greater temporal resolution from continuous, high-sedimentation-rate sections is critical for constructing an ordered timeline of the extinction event and placing local changes in a global context.

The Penglaitan Northern Bank section (Shen et al., 2007) provides a unique opportunity to investigate the period leading up to the EPME at

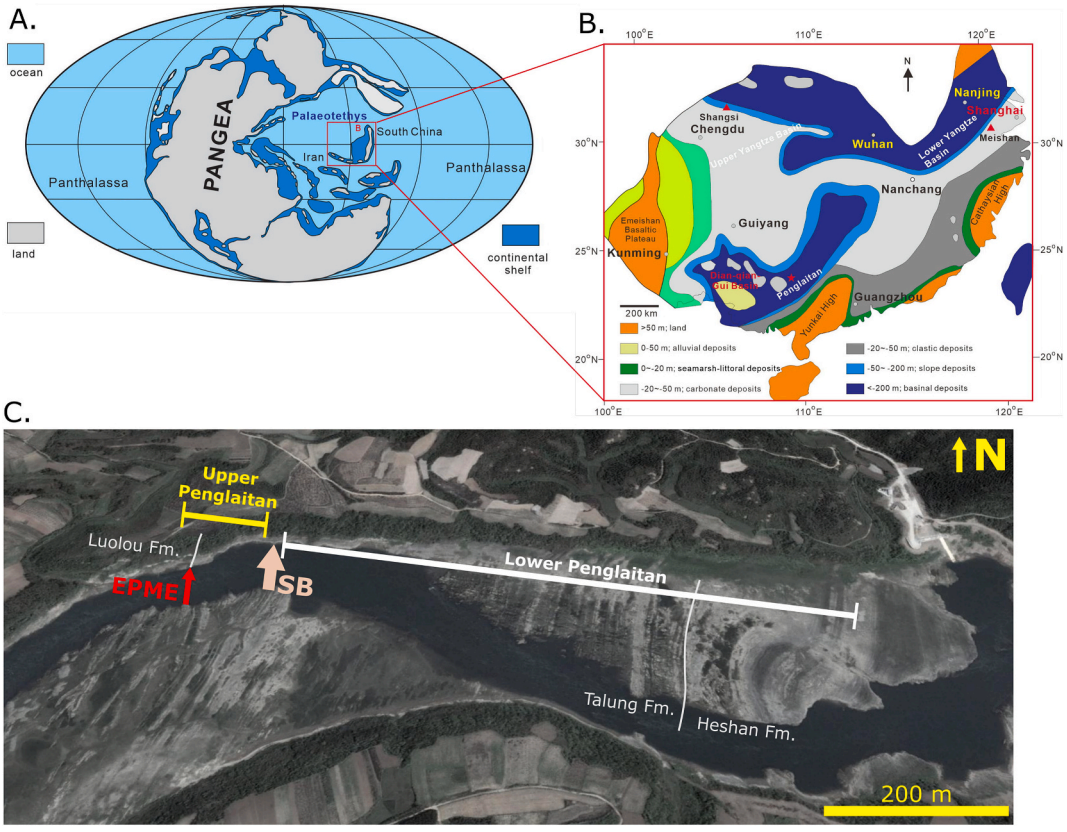

Fig. 1. A. Paleomap showing the location of the South China Block in the latest Permian world. B. Geologic map of the South China Block, in modern orientation, showing depositional facies in the latest Permian and earliest Triassic. C. Google Earth image showing the Penglaitan Northern Bank section (23.69639 N, 109.31688 E), highlighting the Upper and Lower Penglaitan subsections. Imagery is from 2012, prior to major flooding of the section. SB: Sequence Boundary. EPME: end-Permian Mass Extinction.

an unprecedented level of temporal resolution. The section experienced extremely rapid sedimentation throughout the Changhsingian, with over 600 m of strata representing a range of marginal marine and terrestrial environments. Throughout this interval, the Penglaitan depositional environment was impacted by volcanism along the subduction margin of the South China Block (Fig. 1; Zhong et al., 2013). The EPME in this section coincides with ~3 m of tuffaceous sandstone beds. Strata immediately below these beds contain diverse marine fauna, indicating that the extinction, as reflected in this specific environment, was a geologically sudden event, taking place over 31 ± 31 kyr (Shen et al., 2019).

The section at Penglaitan provides a unique opportunity to investigate the interaction between local disruptions to the environment operating on ecological timescales, and the global-scale oceanographic changes associated with the EPME. This study will assess whether changes to the nitrogen cycle, a known feature of the EPME, occurred over a more prolonged timescale than the geologically rapid paleontological extinction at Penglaitan, and whether changes in the nitrogen cycle coincided with, and possibly contributed to, the local disappearance of Permian taxa.

2. Geologic setting and sea level

The Penglaitan section is part of the Laibin Syncline and is exposed along the banks of the Hongshui River, in the Guangxi autonomous region of southern China. While the exposure on the southern bank of the river contains the GSSP for the Guadalupian-Lopingian boundary, the northern bank contains a continuous succession of Late Permian (Lopingian) strata up to the Permian-Triassic Boundary, and extending into the earliest Triassic (Shen et al., 2007; Shen et al., 2019).

The Late Permian interval of the Penglaitan Northern Bank section consists of the uppermost part of the Heshan Formation and the entire overlying Talung Formation, with the formation contact coinciding with the Wuchiapingian-Changhsingian boundary. The Talung Formation spans the Changsingian and is divided into the thin, basal Ergou Member and extensive Penglaitan Member. The contact between the Talung Formation and the overlying Luolou Formation marks the Permian-Triassic Boundary (PTB), the base of the Mesozoic system in South China. The Talung Formation is characterized by carbonate-clastic turbidites and interbedded tuff and tuffaceous sandstone (Fig. 2A) which are interpreted as an overall shallowing upward sequence from ramp-slope to deltaic environments (Shen et al., 2019). These sediments were deposited in the Nanpanjiang Basin, an embayment along the southern margin of the South China Block (Lehrmann et al., 2003, 2005).

High precision U—Pb zircon geochronology indicates an age of 252.359 ± 0.038 Ma in the basal Penglaitan member and an age of 251.991 ± 0.029 Ma just above the late Changhsingian sequence boundary. This is supported by an additional age of 251.931 ± 0.021 Ma at the Penglaitan Mbr.-Luolou Fm. contact (i.e., the EPME; Shen et al., 2019). These ages suggest that 500 m of strata were deposited in ~350–400 kyr. This high sedimentation rate (>1 m/kyr) may be linked to tectonic subsidence and an abundance of siliciclastic and pyroclastic sediment input (Shen et al., 2019).

Terrestrial strata, with sandstones and shales containing fossils of an apparently healthy tropical Permian flora dominated by *Gigantopteris*, appear in the upper Penglaitian Member, ~95 m below the PTB, indicating a conformable sequence boundary. This roughly 40 m interval of terrestrial deposition ended when the environment was submerged by the latest Permian transgression (Lucas and Shen, 2018). This sequence boundary is widely recognized across South China (Yin et al., 2014; Yuan et al., 2014), including at the Meishan section (Xiang et al., 2020). In some literature (e.g., Yin et al., 2014), these strata are referred to as a shelf margin systems tract, due to the continuous deposition of shallow marine strata across the sequence boundary. However, we follow more recent literature (Lucas and Shen, 2018; Shen et al., 2019; Henderson et al., 2020) in interpreting this as a global transgression beginning in the latest Permian.

At Penglaitan, these latest Permian transgression sediments are represented by a 56 m thick, heterolithic succession of thinly-bedded calcareous shales, limestones, and dolostones (Fig. 2B) interbedded with massive volcanogenic sandstones (Fig. 2C), a style of deposition

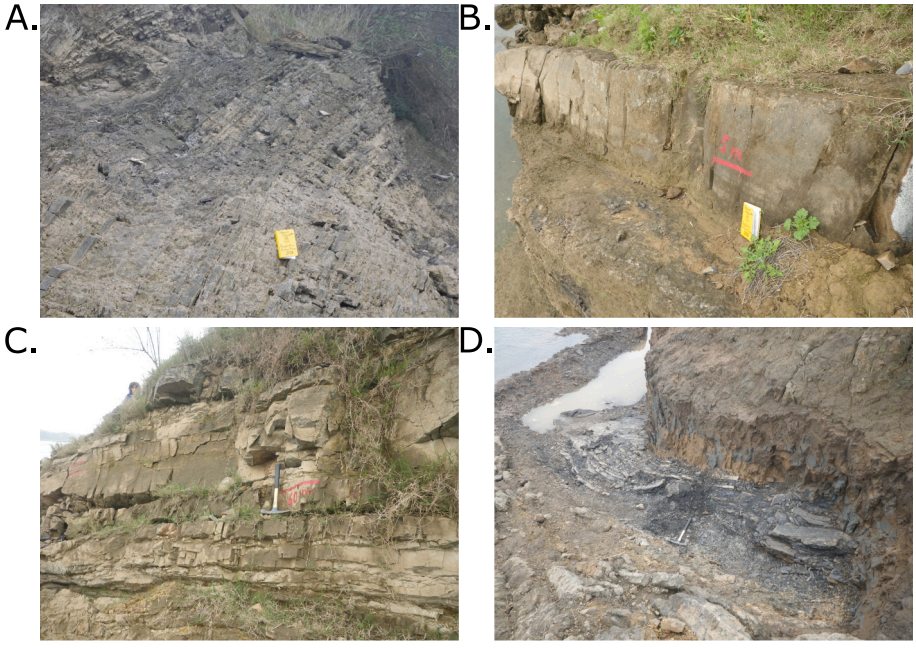

Fig. 2. Photos of the Lower and Upper Penglaitan sections:
A. Representative bedded limestone strata from the Talung Formation, Lower Penglaitan.
B. Sandstone representing the initial transgression of marine waters into the Upper Penglaitan depositional basin.
C. Massive tuffaceous sandstones immediately underlying the EPME in the Upper Penglaitan section.
D. The EPME horizon in the Upper Penglaitan section, recognizable as a sudden transition to black, organic-rich limestones.

that continues up the PTB. This interval of marine deposition is referred to as Upper Penglaitan. Radioisotopic dating of the post-transgression Permian interval at Penglaitan suggests a duration of less than 100 kyr (Shen et al., 2019), which at more typical marine sedimentation rates would be represented by only a few m of strata.

Only a thin interval of earliest Triassic strata are exposed in outcrop, composed of fissile black shales intercalated with cm-scale limestone beds (Fig. 2D). To better understand the Triassic evolution of the basin despite this poor outcrop exposure, the Nanjing Institute of Geology and Palaeontology, Chinese Academy of Sciences (NIGPAS) drilled a 9 cm diameter, 300 m core of the earliest Triassic and latest Permian strata in 2016. This core has been examined in detail and can be correlated with the outcrop section based on two distinct and readily recognizable horizons (both of which also correspond with isotopic shifts, see below). These are the Permian-Triassic Boundary (marked by the top of a ~ 3 m thick interval of tuffaceous sandstone beds), and the latest Permian transgression, above the interval of terrestrial sedimentation. The interval between these benchmarks has the same thickness (~52 m) in the core as in the outcrop section, indicating broadly similar sedimentation rates across the small area of the depositional basin.

3. Methods

3.1. Sample collection

A set of 183 outcrop samples was collected in the field from the Penglaitan Northern Bank section in March 2013. The collected samples are tied to the stratigraphic framework for the section published in Shen et al. (2019), and subsequent publications such as Xiang et al. (2022), with stratigraphic heights marked directly on the outcrop. A total of 88 samples were collected from the Lower Penglaitan part of the section, covering 495 m of strata at approximately 5 m intervals, with some inconsistent spacing to avoid covered intervals or sample unique lithofacies. A total of 95 samples were collected from the Upper Penglaitan section, covering 63.8 m at generally 0.5 m to 1.0 m intervals, with 10 cm intervals approaching the EPME horizon and in the lowermost Triassic.

These outcrop samples were supplemented by material collected from the Penglaitan core described in Section 2. A total of 71 powdered bulk samples from the core, mostly overlapping with the Upper Penglaitan outcrop section, were processed for organic isotope analysis. A larger set of 160 samples, spanning from the Lower Penglaitan interval up into the Lower Triassic, was processed for kerogen extracts (see Section 3.2 below).

3.2. Geochemical measurements

3.2.1. Sample preparation

The data collected for this study consists of four sample sets, measured at a set of collaborating institutions: 1) Upper Penglaitan outcrop samples were processed at the University of Washington (UW), while 2) Lower Penglaitan outcrop samples and 3) bulk core samples were processed at Western Carolina University (WCU) before being measured at the Alabama Stable Isotope Laboratory (ASIL); 4) Core samples for kerogen extraction were processed at NIGPAS.

Sample processing and measurement procedures were similar across all sample sets. Outcrop collected samples were first cleaned manually to remove surface contamination, then broken into small pieces to avoid veins and surface weathering. Samples were cleaned by sonication in ethanol for 1 h, followed by sonication in ultrapure deionized water (>18 MΩ) for 1 h, followed by three consecutive 10-min sonication treatments with deionized water. Samples were then powdered using an agate ball mill (UW) or Spex ShatterBox rock crusher with an alumina ceramic insert (WCU).

In order to simultaneously measure nitrogen and organic carbon isotopes without interference from carbonate, powders were acidified overnight in an excess of 6 N hydrochloric acid solution at >40 °C, then rinsed three times with deionized water before being dried overnight at >40 °C. The percentage of carbonate in each sample was calculated from the difference in sample mass after acidification. Acidification via the rinse can lead to the loss of some soluble organic nitrogen (King et al., 1998; Komada et al., 2008; Fujisaki et al., 2022), which may influence isotope ratios. However, the effect of varying acid concentration is relatively small, particularly at lower temperatures (generally <1 ‰ at room temperature; Fujisaki et al., 2022). Furthermore, all samples were exposed to the same concentration of HCl (6 N). The lack of a relationship between TOC or TN content and isotope values (see below) suggests acidification did not have a systematic effect on nitrogen isotope ratios.

All stable isotope ratios are presented in delta (δ) notation, with atmospheric air as the standard for $\delta^{15}N$ and Vienna PeeDee Belemnite as the standard for $\delta^{13}C_{org}$. Weight percentages of carbon and nitrogen were measured in the course of isotopic analysis, and corrected for the loss of carbonate during the acidification process.

3.2.2. Upper Penglaitan outcrop section

Organic carbon and nitrogen isotopes for the Upper Penglaitan outcrop section (Supplementary Table 1) were measured via elemental-analyzer continuous-flow isotope ratio mass spectrometry (EA-CF-IRMS) at the UW IsoLab facility. An amount of acidified powder sufficient to yield a mass 28 peak area of >25 Vs was weighted into a tin capsule. Depending on the organic content of the sample after acidification, this ranged from 18 to 348 mg of sample powder. Capsules were combusted in a Costech ECS 4010 Elemental Analyzer, coupled to a ThermoFinnegan 253 mass spectrometer through a ThermoFinnegan CONFLO III gas interface. Measurements were corrected using three calibrated internal laboratory standards: glutamic acid 1 ($\delta^{15}N = -4.6$ ‰, $\delta^{13}C_{org} = -28.3$ ‰), glutamic acid 2 ($\delta^{15}N = -5.7$ ‰, $\delta^{13}C_{org} = -13.7$ ‰), and salmon tissue ($\delta^{15}N = +11.3$ ‰, $\delta^{13}C_{org} = -21.3$ ‰). The average analytical precision based on repeated measurement of organic standards was ±0.11 ‰ for nitrogen and ± 0.31 ‰ for organic carbon.

3.2.3. Lower Penglaitan Outcrop section and bulk core samples

Carbon and nitrogen isotopes for the Lower Penglaitan outcrop section (Supplementary Table 2) and bulk core samples (Supplementary Table 3) were measured via EA-CF-IRMS at the Alabama Stable Isotope Laboratory. An amount of acidified powder sufficient to yield a mass 28 peak area of >12 Vs was weighted into a tin capsule. Depending on the organic content of the sample after acidification, this ranged from 40 to 55 mg of sample powder. Capsules were combusted in a Costech 4010 Elemental Combustion System, coupled to a Thermo Delta V Plus mass spectrometer in continuous flow mode. Measurements were corrected using two standard materials for nitrogen and one for organic carbon: B2153 low organic soil ($\delta^{15}N = +5.8$ ‰, $\delta^{13}C_{org} = -22.9$ ‰), and USGS25 ammonium sulfate ($\delta^{15}N = -30.4$ ‰). The average analytical precision based on repeated measurement of organic-containing sediment standards was ±0.42 ‰ for $\delta^{15}N$ and ± 0.18 ‰ for $\delta^{13}C_{org}$.

3.2.4. Kerogen Extracts from core

A total of 160 samples from the Penglaitan core were broken into small pieces (diameter ~ 2 mm) by hammer at NIGPAS. Individual pieces were selected to avoid fracture fills, veins, and nodules, and powdered using a SPEX 8515 Shatterbox with a ceramic insert. Samples were prepared following Cai et al. (2009), and Kump et al. (2011); powders were treated with 6 N HCl, then a mixture of 6 N HCl and 40 % HF, followed by a final treatment with 6 N HCl, to remove carbonate and silicates. The residue was rinsed in distilled water, centrifuged and dried. Measured C:N ratios of the organic residues were scaled to the TOC content of the original sample, to calculate the abundance of kerogen-bound nitrogen.

Total nitrogen content and the nitrogen isotope composition of organic residues were both measured using a modified elemental

analysis-isotope ratio mass spectrometry (EA-IRMS) procedure (CEEA1112 CNS Analyzer, interfaced with a DELTA plus XL mass spectrometer), at the Guangzhou Institute of Geochemistry, Chinese Academy of Sciences. The details of this method and the analytical system are described in Li and Jia (2011). Measurements were corrected using four standard materials: USGS34 potassium nitrate ($\delta^{15}N = -1.8$ ‰), IAEA NO-3 potassium nitrate ($\delta^{15}N = +4.7$ ‰), IAEA N1 ammonium sulfate ($\delta^{15}N = +0.4$ ‰), and IAEA N2 ammonium sulfate ($\delta^{15}N = +20.3$ ‰). Results are reported in standard delta notation, relative to atmospheric air. Reproducibility was ±0.5 ‰ for $\delta^{15}N$.

4. Results and discussion

4.1. Organic material

TOC is generally low, and relatively consistent, throughout the Lower Penglaitan section, ranging from 0.10 to 1.67 wt% (Fig. 3; mean = 0.43 %, standard deviation = 0.21 %). Values are slightly lower on average in outcrop material from the Upper Penglaitan section (mean = 0.28 %, standard deviation = 0.85 %), though one outlying point shows a TOC value of 8.18 %. TOC in the core material is generally higher (mean = 0.57 %, standard deviation = 0.41 %), with sporadic elevated values reaching as high as 1.77 % (Fig. 3). The higher TOC content in core samples relative to outcrop samples where the two datasets overlap suggests diagenetic loss of carbon in outcrop samples relative to subsurface material. The potential effects of diagenetic carbon loss on $\delta^{15}N$ values are considered below.

Total nitrogen content is more consistent in the three datasets (Fig. 3), with a mean value of 0.05 wt% (standard deviation = 0.02 %) in the Lower Penglaitan section, 0.03 wt% (standard deviation = 0.02 %) in Upper Penglaitan outcrop samples, and 0.04 wt% (standard deviation = 0.02 %) in core material (Fig. 3). The linear relationship between TOC and TN is consistent between the Upper Penglaitan and Lower Penglaitan outcrop sections, with most core samples also falling on this same trend (Fig. 4A). This indicates that most nitrogen is hosted in marine organic material, rather than bound to clays or other silicates. Core and Lower Penglaitan samples showing TOC values to the right of the trendline (corresponding to higher C:N ratios, see below) likely represent a component of terrestrial organic matter in the system.

Organic Carbon to nitrogen ratios (wt./wt.) range over an order of magnitude, from 3.0 to 46.7, in the Lower Penglaitan section (Fig. 3; mean = 10.1, standard deviation = 6.3). The Upper Penglaitan section has a similar mean value of 10.3 but more variable C:N ratios (standard deviation = 9.9), with maximum values as high as 87.2. Core material has both higher mean (21.4, standard deviation = 28.4) and higher maximum values (149.5) than outcrop samples. Elevated C:N ratios of organic matter (>20 wt./wt.) are seen in the lowermost Penglaitan Member, and even higher ratios, above 50, are seen exclusively in the Upper Penglaitan part of the section, and almost exclusively in core material (Fig. 3).

While high C:N ratios generally occur with TOC values above 0.5 wt %, there is no clear relationship between TOC and C:N ratios (Fig. 4B), suggesting that enhanced preservation of carbon in core material is not the sole explanation for these elevated values. High C:N ratios likely record short-lived influxes of terrestrial organic matter (Meyers, 1994), initially during deposition of the lowermost Penglaitan Member, where

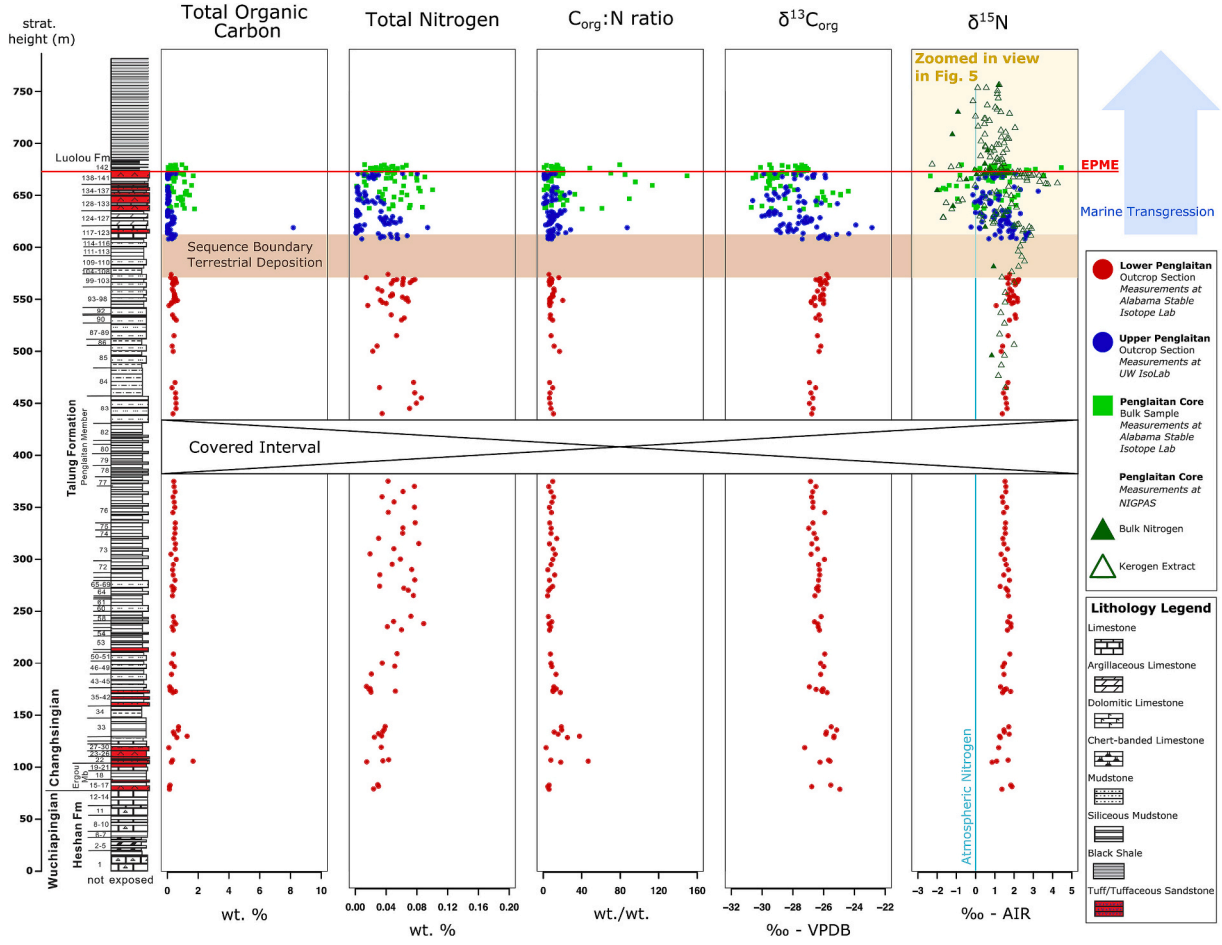

Fig. 3. Stratigraphic column of the Penglaitan North Bank outcrop section and associated core, showing organic geochemical and isotope data. See Fig. 5 for lithology legend. Stratigraphic column modified from Shen et al., 2019.

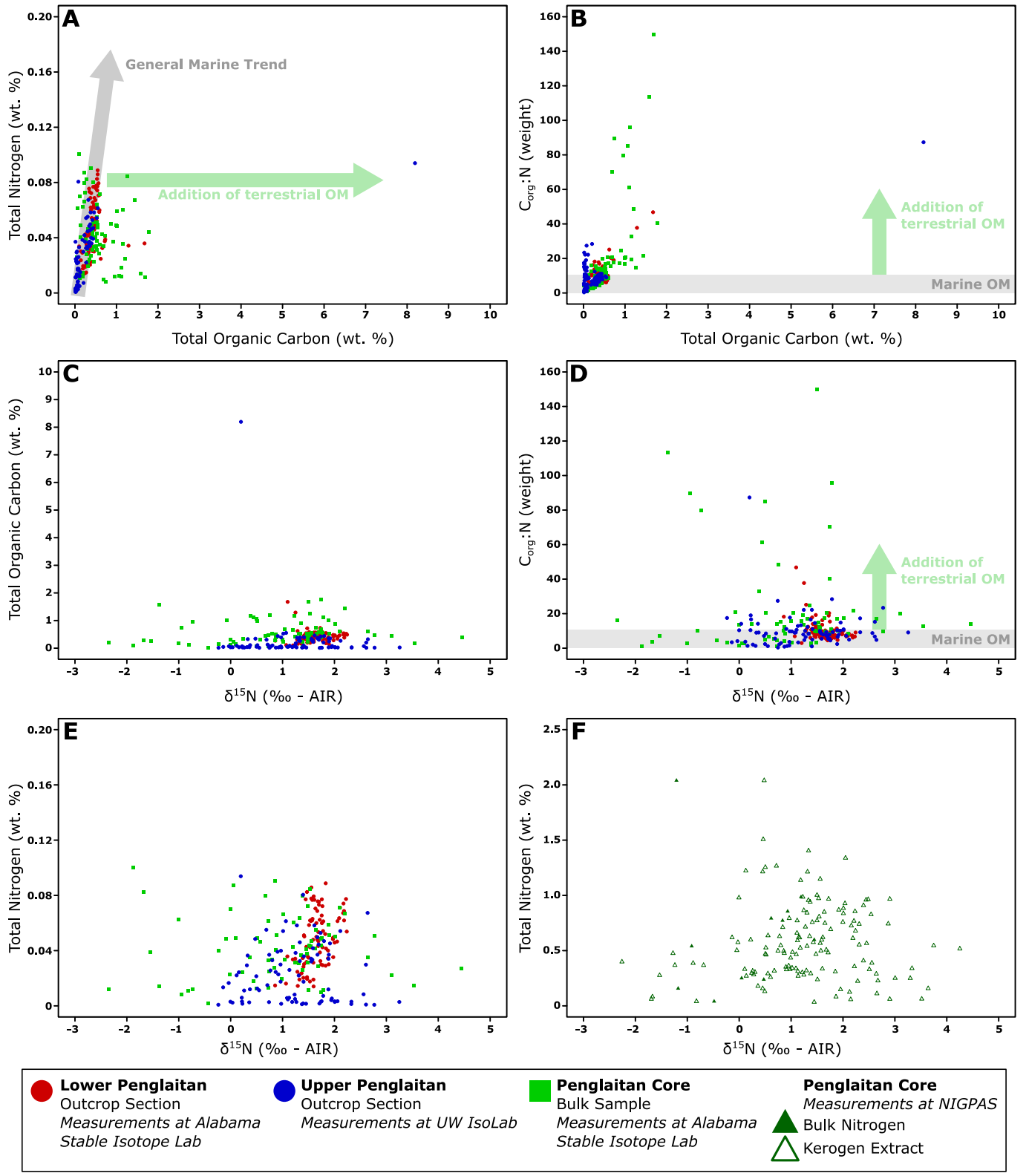

Fig. 4. Crossplots of organic geochemical data from the Penglaitan Northern Bank outcrop section and core. A C:N ratio of 10, used as the threshold between marine and terrigenous organic matter in Panels 4B and 4D, is derived from Meyers (1994). This value also corresponds closely with the mean C:N ratio of Penglaitan samples, as seen in Panel 4 A.

A. Total organic carbon (wt%) vs. Total nitrogen (wt%).
B. Total organic carbon (wt%) vs. Carbon to nitrogen ratio (by weight).
C. $\delta^{15}N$ (‰ - AIR) vs. Total organic carbon (wt%).
D. $\delta^{15}N$ (‰ - AIR) vs. Carbon to nitrogen ratio (by weight).
E. $\delta^{15}N$ (‰ - AIR) vs. Total nitrogen (wt%) in bulk rock samples.
F. $\delta^{15}N$ (‰ - AIR) vs. Total nitrogen (wt%) in kerogen extracts.

they correspond to lignitic shale deposits containing ammonoids, and again during deposition of the Upper Penglaitan section. This interpretation is reinforced by the presence of coal beds and fossils of the *Gigantopteris* flora in the sequence boundary interval prior to the latest Changhsingian transgression (Shen et al., 2007), indicating the presence of lush, productive terrestrial forests persisting on the margins of the depositional environment into the latest Permian.

It is reasonable to ask whether $\delta^{15}N$ values are affected by diagenetic loss of organic material or differential ratios of marine and terrestrial organic material in the section. $\delta^{15}N$ values are not strongly influenced by overall organic content, with the highest TOC samples (typically core material) showing a full range of $\delta^{15}N$ values (Fig. 4C). Almost the full range of observed $\delta^{15}N$ values can be seen in samples with low C:N ratios consistent with marine organic matter, while samples with elevated C:N ratios (almost exclusive to core material) tend to have modal $\delta^{15}N$ values (Fig. 4D). This suggests that, to the extent that outcrop samples had higher initial C:N ratios that have been modified by diagenetic loss of terrestrial organic matter, these terrestrial sources did not exert a strong directional influence on $\delta^{15}N$ values in marine sediments.

There is no systematic relationship between total nitrogen content and $\delta^{15}N$, either in bulk material (Fig. 4E) or kerogen extracts (Fig. 4F), suggesting that $\delta^{15}N$ values were not strongly influenced by either diagenetic loss of nitrogen, or loss of soluble organic matter during acidification. Taken together, these results indicate that measured $\delta^{15}N$ values in both outcrop and core material primarily reflect syndepositional nitrogen cycle processes, rather than preservational signals.

4.2. Carbon isotope geochemistry

$\delta^{13}C_{org}$ in the Talung Formation show a high degree of stability below the latest Permian transgression. Values range from −27.2 to −25.0 ‰, with a mean of −26.3 ‰ and a standard deviation of 0.44 ‰. This stability is evident despite the elevated C:N ratios in parts of the Ergou Member and lowermost Penglaitan Member, suggesting that terrestrial organic matter was a minor component of the overall OM pool, or that terrestrial OM did not differ isotopically from marine OM in adjacent environments in this interval.

$\delta^{13}C_{org}$ is considerably more variable above the terrestrial interval, following the latest Permian transgression. The range of variation seen in outcrop material (−30.6 to −22.9 ‰, mean = −27.8 ‰, standard deviation = 1.53 ‰) does not differ greatly from that seen in core material (−30.7 to −24.4 ‰, mean = −28.0 ‰, standard deviation = 1.50 ‰) despite the substantially higher TOC values seen in some core samples. The highest $\delta^{13}C_{org}$ values in the section (up to −23 ‰) are seen in outcrop material from just above the Upper Penglaitan transgressive surface. This is consistent with measurements from Shen et al. (2019), who attributed this and other brief positive excursions in $\delta^{13}C_{org}$ in the Upper Penglaitan section to the mixing of terrestrial and marine organic material, with fluxes of terrestrial organic carbon likely driven by episodes of volcanic activity.

Focusing specifically on the Triassic interval of the core material, the average $\delta\ ^{13}C_{org}$ value is −27.9 ‰ (standard deviation = 0.91 ‰), not significantly different from that seen during the latest Permian transgression. This decrease in $\delta\ ^{13}C_{org}$ values, by approximately 2 ‰, represents the local expression of the negative $\delta^{13}C_{org}$ shift seen globally in this interval (Korte and Kozur, 2010). It is notable that this transition corresponds to the latest Permian transgression, rather than the EPME or PTB horizon, and that it represents an expansion of carbon isotope variability rather than simply a monotonic decrease. Both of these observations are also true of $\delta^{13}C_{carb}$ measurements at Penglaitan (Shen et al., 2019) These aspects are likely to be less evident in more stratigraphically condensed sections, such as the PTB GSSP at Meishan (Yuan et al., 2014), where the sequence boundary preceding latest Permian transgression is located at the base of the *Clarkina meishanensis* Zone (Yin et al., 2014), less than 2 m below the PTB. In many sections it may be difficult to effectively distinguish the onset of transgression from the PTB without high-resolution sampling.

4.3. Nitrogen isotope geochemistry

$\delta^{15}N$ data from Penglaitan strongly indicate nitrogen cycle stability throughout most of the Changhsingian. Values from the Lower Penglaitan interval (i.e., the Talung Formation below the interval of terrestrial deposition) show very little variation in nitrogen isotope values), ranging from 0.9 to 2.2 ‰ with an average of 1.6 ‰ and a standard deviation of 0.3 ‰. Bulk nitrogen isotope measurements from outcrop are highly consistent with kerogen extracts from the core in this interval (Fig. 3).

While lower than the average modern marine nitrate value of 5 ‰ (Sigman et al., 2000), these values are typical of the later Paleozoic, and more generally of 'greenhouse' periods of Earth history (Kidder and Worsley, 2010; Algeo et al., 2014). These values also seem to be typical for terrestrial organic matter in this setting. Lignitic shales from the upper Ergou Member and lower Penglaitan member, with C:N ratios >20 suggesting a significant component of terrestrial organic matter (Meyers, 1994), yield $\delta^{15}N$ values ranging from 1.0 to 1.5 ‰, consistent with stratigraphically adjacent marine sediments.

These Changhsingian $\delta^{15}N$ values, slightly but consistently above 0 ‰, reflect cycling of fixed nitrogen influenced by the oceanographic conditions of a 'greenhouse' climate regime as defined by Kidder and Worsley (2010), characterized by a lack of polar ice, sluggish ocean circulation, and extensive sedimentary denitrification (Algeo et al., 2014). The oceans warmed rapidly in the latest Permian and earliest Triassic, with the tropical surface ocean reaching temperatures greater than 35 °C (Sun et al., 2012; Romano et al., 2013). Conodont apatite paleotemperatures from the Penglaitan section reach values >40 °C in the earliest Triassic (Shen et al., 2019). These warm temperatures would have promoted stratification of the water column (Song et al., 2012).

Under conditions of sluggish ocean circulation, nitrate regenerated from decomposing organic matter is more likely to be denitrified in suboxic to anoxic water masses, and have a shorter residence time in the ocean. The lack of fixed N availability can be compensated for by intensified N fixation, which brings new, bioavailable N into the ocean system with a $\delta^{15}N$ of ~0 ‰ (Zhang et al., 2016). At the same time, during intervals of high sea level, a greater proportion of denitrification is likely to take place in the suboxic sediments of flooded continental shelves, where nitrate trapped in pore water can be completely denitrified, with no fractionation effect (Algeo et al., 2014). Both of these processes were likely broadly prevalent in the Changhsingian ocean, with the organic rich sedimentary basins of the flooded South China Block likely serving as an especially favorable site for denitrification. While bottom waters at Penglaitan remained predominantly oxic in this interval (Xiang et al., 2022), the stability of both organic carbon and nitrogen isotope signals across major facies changes at Penglaitan (see below) suggests that isotope signals may reflect broader regional trends.

$\delta^{15}N$ values from the terrestrial interval, represented exclusively by kerogen extracts of core material, are only slightly elevated above those in the Lower Penglaitan marine section (mean = 2.1 ‰, standard deviation = 0.4 ‰; Fig. 3). This is true despite the presence of a fossil *Gigantopteris* flora, likely the source for much of the organic nitrogen in this interval. As with the the lignitic shale interval in the early Changhsingian, the lack of isotopic variation suggests that terrestrial primary producers had broadly similar nitrogen isotope values to marine algae in this system.

This inference is supported by samples with high C:N ratios generally having modal $\delta^{15}N$ values (Fig. 4D). Outcrop samples from Upper Penglaitan with C:N ratios greater than 10 (and thus inferred to contain a substantial component of terrestrial organic matter, see Meyers, 1994) have a similar mean (1.1 ‰) and range of variation (−0.2 to 2.8 ‰) to samples with more typically marine C:N ratios of less than 10 (−0.1 to 3.3 ‰, mean = 1.2 ‰). In core material from Upper Penglaitan, samples with C:N ratios greater than 10 show a greater range of variation (−2.3

to 4.5 ‰) than samples with C:N ratios below 10 (−1.9 to 2.8 ‰). While the highest $\delta^{15}N$ values (>3.0 ‰) are only seen in samples with elevated C:N ratios, those samples with the highest C:N ratios (>50) show modal $\delta^{15}N$ values ranging from −1.5 to 2.0 ‰ (Fig. 4D). Given these observations, it is likely that the continued flux of terrestrial organic matter contributed to the increased variability in $\delta^{15}N$ in the Upper Penglaitan section even after the resumption of marine deposition, but did not have a clear directional effect on nitrogen isotopes.

Values in the Upper Penglaitan outcrop section range from −0.2 to 3.3 ‰, with a mean of 1.2 ‰ and a standard deviation of 0.7 ‰. Bulk values from the core range from −2.4 to 4.5 ‰, with a mean of 0.9 ‰ and a standard deviation of 1.2 ‰. This increased variability above the latest Permian transgression is also seen in kerogen extracts, with range from −1.7 to 4.3 ‰ in this interval, with a mean of 1.4 ‰ and a standard deviation of 1.4 ‰. The first appearance of values near or below 0 ‰, seen primarily in samples with low C:N ratios, suggests that nitrogen fixation was at times the dominant source of nitrogen to the marine environment. At the same time, $\delta^{15}N$ values well above those typical in the Lower Penglaitan section suggest periodic influxes of terrestrial organic material, and/or an increasing role of water column denitrification. Iron speciation results (Xiang et al., 2022) indicate predominantly oxic conditions in the depositional basin during this interval, which is consistent with the continued deposition of carbonates containing a diverse fauna (Shen et al., 2019). Water-column denitrification, which does not appear persistent in the isotope record, may have occurred during short-lived incursions of ferruginous, denitrifying water masses into the Penglaitan slope setting (Fig. 6), as recognized by Xiang et al. (2022).

Nitrogen fixation can occur in response to oligotrophy (a lack of available nutrients; c.f. Luo et al., 2011), or when other nutrients such as iron or phosphorus are available in excess relative to nitrogen, likely due to enhanced weathering (Algeo et al., 2011; Schobben et al., 2015).

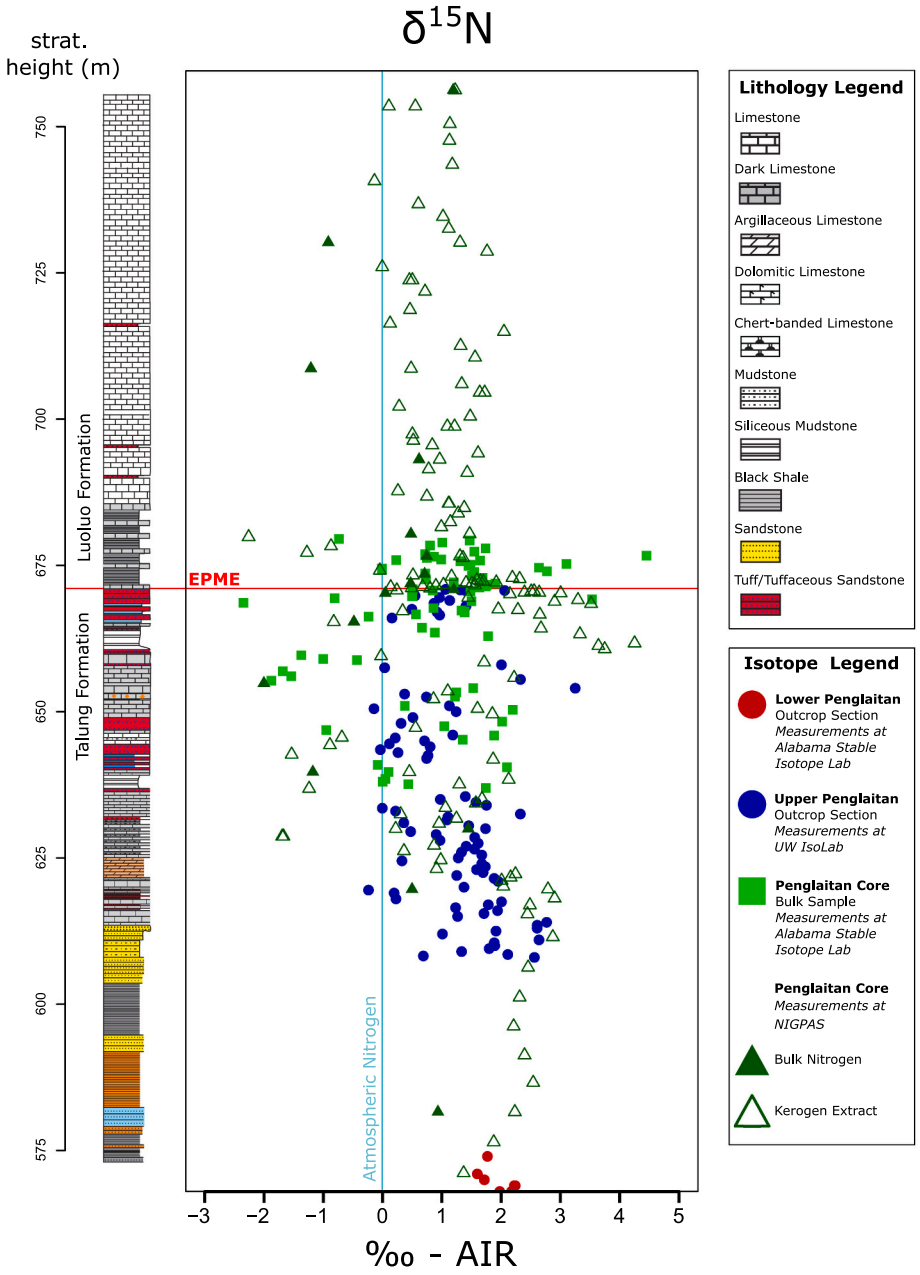

Fig. 5. Stratigraphic column of the Upper Penglaitan outcrop section and associated core, showing nitrogen isotope data. Stratigraphic column modified from Shen et al., 2019.

Values lower than −1.0 ‰ occur primarily (though not exclusively) in carbonate-dominated facies at Penglaitan, in both the latest Permian and earliest Triassic (Fig. 5). With isotopic evidence for intense N fixation in authigenic carbonates rather than siliciclastic beds, it is reasonable to conclude that these intervals were oligotrophic, with diazotrophs responding to limited N availability in the surface ocean. Low primary productivity is associated with clear water, allowing for deposition of carbonates containing a diverse fauna (Brasier, 1995a, 1995b), which is observed at Penglaitan even in beds immediately underlying the end-Permian extinction horizon (Shen et al., 2019).

While predominantly seen in carbonates, the extremely low $\delta^{15}N$ values indicating nitrogen fixation are seen in a range of carbonate textures, from more thinly bedded argillaceous beds appearing just above the latest Permian transgression, to massive limestones in the uppermost Talung Formation. The lack of a clear relationship to facies suggests that nitrogen fixation was not a local signal but represents a response by the oxic surface ocean to widespread regional denitrification happening primarily in deeper water oxygen minima. It is worth noting that some of the *highest* values of $\delta^{15}N$ in this interval (measured in kerogen extracts from the core) correspond to a black shale interval from 660 to 664 m (Fig. 5), which may correspond with either a) a discrete influx of terrestrial organic material, or b) a specific incursion of deeper anoxic waters into this shallow environment (Riccardi et al., 2006; Song et al., 2012; Xiang et al., 2022). These potential explanations need not be mutually exclusive, as an incursion of anoxic waters would tend to enhance organic carbon preservation, while an influx of exogenous organic material from coastal environments could fuel oxygen demand, driving the system toward anoxia.

The earliest Triassic section, represented solely by core material, has a mean $\delta^{15}N$ of 1.3 ‰ (standard deviation = 1.1 ‰) in bulk samples, which only include the lowermost 5 m of the Triassic. Kerogen extracts from the Triassic section, spanning over 80 m of strata, have a mean $\delta^{15}N$ of 0.8 ‰ (standard deviation = 0.8 ‰). While values generally show a smaller range of variability than is seen in the latest Permian Upper Penglaitan interval, suggesting some stabilization of the nitrogen cycle after the immediate extinction interval (Fig. 5), mean $\delta^{15}N$ values are lower and standard deviations are higher than those seen in the Lower Penglaitan section; clearly the earliest Triassic did not represent a return to pre-extinction baseline conditions. These lower values are consistent with previous findings of persistent oligotrophy well into the Early Triassic (Grasby et al., 2016; Du et al., 2023), which did not begin to alleviate until the Spathian substage.

A transition to lower nitrogen isotope values around the Permian-Triassic boundary is seen across a variety of marine environments (Luo et al., 2011; Schoepfer et al., 2012; Knies et al., 2013; Algeo et al., 2014; Grasby et al., 2016, 2020; Zakharov et al., 2021; Schoepfer and Henderson, 2021; Du et al., 2023). The trend seen at Penglaitan is notable for two reasons. Firstly, like the $\delta^{13}C_{org}$ excursion, the nitrogen cycle transition predates the paleontologically-defined extinction in this environment, albeit likely by <100 kyr. Secondly, the transition to lower nitrogen isotope values is less a discrete state shift than an expansion in the range of values, with $\delta^{15}N$ values of ~0 ‰ becoming increasingly common, while other samples continue to yield values comparable to the Changhsingian baseline or higher.

In more condensed sections, this expanded range of variability is likely to present as a single discrete excursion. When nitrogen isotope data from Penglaitan is averaged by 5 m bins, simulating stratigraphic condensation, it yields a pattern comparable to that seen in other sections across the South China Block (Fig. 7; Luo et al., 2011), though the main excursion can still be seen to significantly predate the extinction. It is worth noting that, even with the resolution offered by the Penglaitan section, the lowest $\delta^{15}N$ values are explicable via N fixation using molybdenum based nitrogenases (Zhang et al., 2016). While some of the lowest values are consistent with direct assimilation of ammonium from deep water (Sun et al., 2019; Du et al., 2023), they do not require it, and the fact that they correspond with geochemical evidence for oxic conditions (Xiang et al., 2022), diverse marine metazoan fauna (Shen et al., 2019), and carbonate deposition consistent with oligotrophy (Brasier, 1995a, 1995b) argue that they do not represent upward excursions of an ammonium ocean.

5. Conclusions

The Penglaitan Northern Bank section shows that the marine nitrogen cycle was characterized by stability throughout most of the Changhsingian stage, with $\delta^{15}N$ values ranging from 0.9 to 2.2 ‰, reflecting a greenhouse regime of widespread sedimentary denitrification (Kidder and Worsley, 2010; Algeo et al., 2014). Nitrogen cycle stability is especially notable given the evidence for repeated disturbance of the local marine environment by volcanic eruptions. Given this apparent stability of the marine nitrogen cycle in a locally unstable environment, nitrogen isotopes at Penglaitan may be primarily reflecting geographic trends across the South China Block, or the broader western Panthalassic Ocean.

This continuity is interrupted after the latest Permian transgression (beginning at approximately 252.0 Ma, Lucas and Shen, 2018), after which the local nitrogen cycle becomes unstable, with $\delta^{15}N$ values ranging from −2.4 to 4.5 ‰. The lowest values are primarily but not exclusively seen in carbonate facies with a diverse fauna, consistent with nitrogen fixation by diazotrophs in response to oligotrophy. The highest values are seen in a black shale unit, which may reflect an influx of terrestrial organic matter, or an upward incursion of the chemocline carrying nitrate impacted by water column denitrification (Xiang et al., 2022). This instability is ameliorated somewhat in the earliest Triassic, though values remain lower than those seen in the pre-extinction Late Permian, which agrees well with other findings that photic zone oligotrophy remained widespread across the South China Block well into the Early Triassic (Luo et al., 2011; Du et al., 2023)

The unusual aspects of carbon and nitrogen cycle records in the Penglaitan Northern Bank section are likely a result of the extremely high sedimentation rate (Shen et al., 2007; Shen et al., 2019). $\delta^{15}N$ values indicate that the start of the Permian-Triassic crisis, when viewed from a nitrogen cycle perspective, coincides with the onset of the latest Permian transgression. Permian faunas are apparent for another 70 m of strata which supports the view that the extinction was likely globally diachronous on the order of tens of thousands of years (Algeo et al., 2012). Indeed, characteristically Early Triassic fauna begin to appear in this transitional interval (Shen et al., 2019).

The sudden extinction of Permian fauna at Penglaitan coincides with a massive tuffaceous sandstone bed, of a type common in the pre-extinction Penglaitan section. Intermediate-scale regional disturbances of the fauna must have been relatively common in volcanically active South China, where diverse seafloor ecosystems were regularly buried under massive crystalline tuffs, only to recolonize the new seafloor surface (Fig. 6; Godbold et al., 2017) – what set the end-Permian extinction apart was that oceanographic conditions had deteriorated to the point of inhibiting this routine recovery. This deterioration began with the latest Permian transgression, and included disrupted nutrient cycling, oligotrophy, repeated incursions of anoxic waters, and the appearance of characteristically Triassic 'disaster taxa' such as *Claraia* (Shen et al., 2019). However, these conditions coexisted with the persistence of characteristically Permian fauna during the final 100 kyr of the Paleozoic, with only the abrupt warming at the Permian-Triassic boundary being sufficient to fully inhibit recovery. This interplay between local ecological dynamics and global biogeochemical processes cannot be easily discerned in lower resolution sections.

CRediT authorship contribution statement

Shane D. Schoepfer: Writing – review & editing, Writing – original draft, Investigation, Funding acquisition, Conceptualization. **Eldridge Machen:** Writing – original draft, Investigation. **Hannah Cothren:**

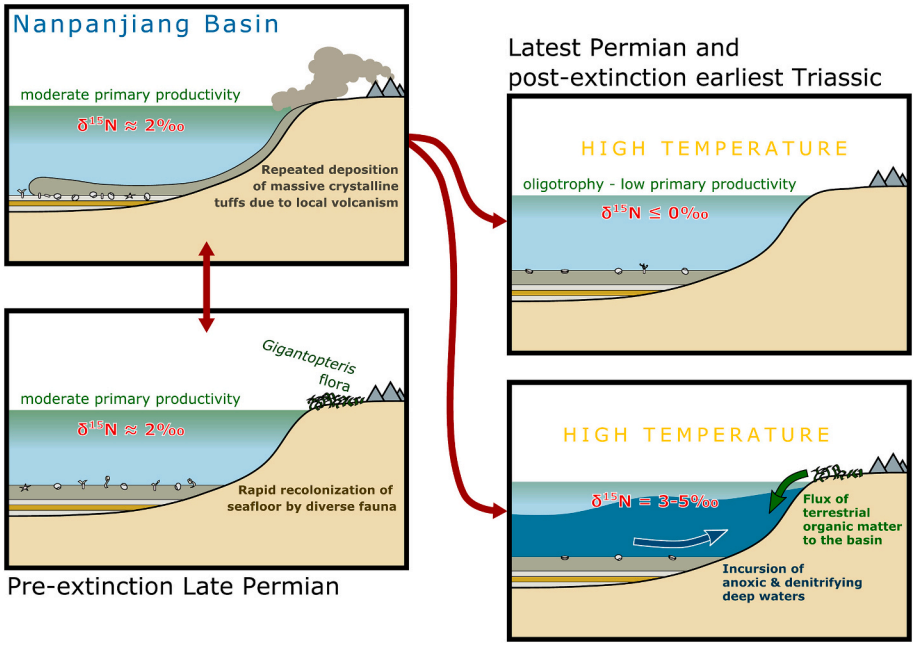

Fig. 6. Model of deposition in the Nanpanjiang Basin, repeatedly punctuated by local volcanism on the subduction margin of the South China Block (Zhong et al., 2013). These local disruptions had no long term effect on ecosystems until the onset of the latest Permian transgression. Note that nitrogen cycle instability occurs in the latest Permian, but high sea surface temperatures appear suddenly at the end-Permian extinction horizon (Shen et al., 2019).

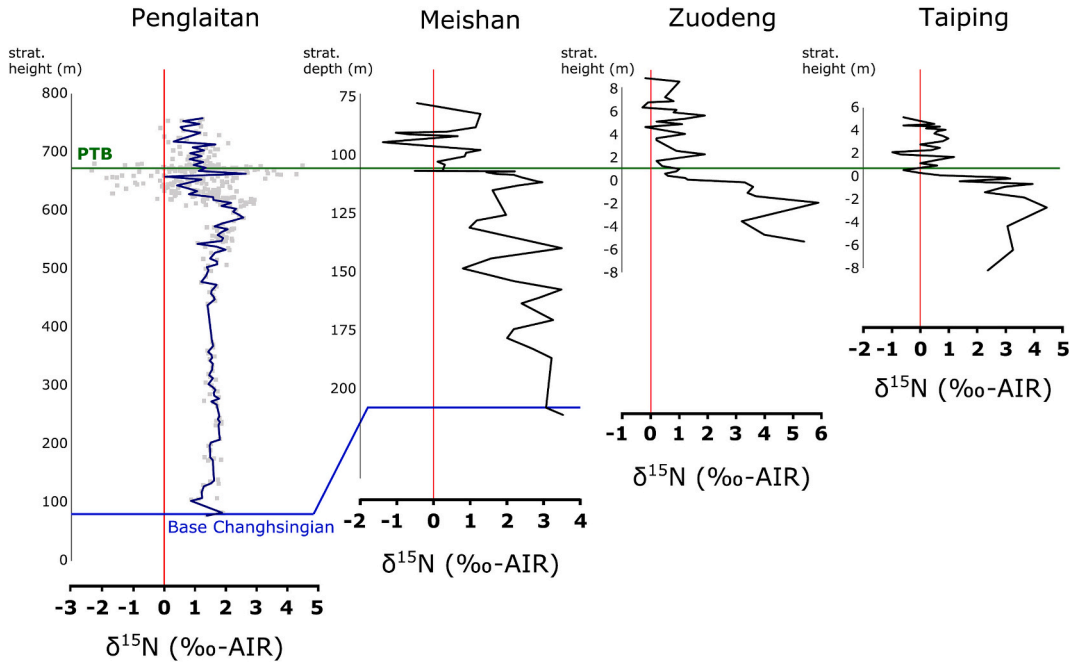

Fig. 7. Comparison of Penglaitan to three other sections from the South China Block. All $\delta^{15}N$ data from this study are shown as gray squares. The dark blue line shows the average values of binned 5 m intervals, simulating the effects of stratigraphic condensation. The Meishan stratigraphic column is vertically exaggerated by a factor of 4 relative to the Penglaitan column. The Zuodeng and Taiping columns are vertically exaggerated by a factor of 10 relative to the Meishan column, and a factor of 40 relative to the Penglaitan column. Penglaitan is correlated to Meishan at the base of the Changhsingian stage, and all sections are correlated by the Permian-Triassic Boundary. Data from Meishan are from Cao et al. (2009). Data from Zuodeng and Taiping are from Luo et al. (2011). (For interpretation of the references to colour in this figure legend, the reader is referred to the web version of this article.)

Writing – review & editing, Writing – original draft, Investigation. **Lei Xiang:** Investigation, Funding acquisition, Conceptualization. **Hua Zhang:** Investigation, Funding acquisition, Conceptualization.

Declaration of competing interest

The authors declare that they have no known competing financial interests or personal relationships that could have appeared to influence the work reported in this paper.

Acknowledgments

The authors would like to extend their gratitude to Dr. Joe Lambert and the staff of the University of Alabama Stable Isotope Laboratory, as well as Andy Schauer and the staff of the University of Washington IsoLab. This work is supported by the National Natural Science Foundation of China (Grants No. 92479206), the National Key Research and Development Program of China (Grant No. 2024YFF0808101), and the Jiangsu Innovation Support Plan for International Science and Technology Cooperation Program (Grant No. BZ2023068). We would also like to thank the State Key Laboratory of Palaeobiology and Stratigraphy grant 183103 to SDS and LX, for providing funding for student travel and fieldwork and to Western Carolina University's Undergraduate Academic Project Grants program for providing funding for the analyses included in this study.

Appendix A. Supplementary data

Supplementary data to this article can be found online at https://doi.org/10.1016/j.gloplacha.2025.104868.

Data availability

All data used in this study is available in Supplementary Tables

References

Aftabuzzaman, M., Kaiho, K., Biswas, R.K., Liu, Y., Saito, R., Tian, L., Bhat, G.M., Chen, Z. Q., 2021. End-Permian terrestrial disturbance followed by the complete plant devastation, and the vegetation proto-recovery in the earliest-Triassic recorded in coastal sea sediments. Glob. Planet. Chang. 205, 103621.

Algeo, T.J., Shen, J., 2024. Theory and classification of mass extinction causation. Natl. Sci. Rev. 11 (1) nwad237.

Algeo, T.J., Twitchett, R.J., 2010. Anomalous early Triassic sediment fluxes due to elevated weathering rates and their biological consequences. Geology 38 (11), 1023–1026.

Algeo, T.J., Chen, Z.Q., Fraiser, M.L., Twitchett, R.J., 2011. Terrestrial–marine teleconnections in the collapse and rebuilding of early Triassic marine ecosystems. Palaeogeogr. Palaeoclimatol. Palaeoecol. 308 (1–2), 1–11.

Algeo, T., Henderson, C.M., Ellwood, B., Rowe, H., Elswick, E., Bates, S., Lyons, T., Hower, J.C., Smith, C., Maynard, B., Hays, L.E., 2012. Evidence for a diachronous late Permian marine crisis from the Canadian Arctic region. GSA Bull. 124 (9–10), 1424–1448.

Algeo, T.J., Henderson, C.M., Tong, J., Feng, Q., Yin, H., Tyson, R.V., 2013. Plankton and productivity during the Permian–Triassic boundary crisis: an analysis of organic carbon fluxes. Glob. Planet. Chang. 105, 52–67.

Algeo, T.J., Meyers, P.A., Robinson, R.S., Rowe, H., Jiang, G.Q., 2014. Icehouse–greenhouse variations in marine denitrification. Biogeosciences 11 (4), 1273–1295.

Benton, M.J., Newell, A.J., 2014. Impacts of global warming on Permo-Triassic terrestrial ecosystems. Gondwana Res. 25 (4), 1308–1337.

Benton, M.J., Twitchett, R.J., 2003. How to kill (almost) all life: the end-Permian extinction event. Trends Ecol. Evol. 18 (7), 358–365.

Bond, D.P., Grasby, S.E., 2017. On the causes of mass extinctions. Palaeogeogr. Palaeoclimatol. Palaeoecol. 478, 3–29.

Brasier, M.D., 1995a. Fossil indicators of nutrient levels. 1: Eutrophication and climate change. Geol. Soc. Lond. Spec. Publ. 83 (1), 113–132.

Brasier, M.D., 1995b. Fossil indicators of nutrient levels. 2: Evolution and extinction in relation to oligotrophy. Geol. Soc. Lond. Spec. Publ. 83 (1), 133–150.

Burgess, S.D., Bowring, S.A., 2015. High-precision geochronology confirms voluminous magmatism before, during, and after Earth's most severe extinction. Sci. Adv. 1 (7), e1500470.

Cai, C., Li, K., Anlai, M., Zhang, C., Xu, Z., Worden, R.H., Wu, G., Zhang, B., Chen, L., 2009. Distinguishing Cambrian from Upper Ordovician source rocks: evidence from sulfur isotopes and biomarkers in the Tarim Basin. Org. Geochem. 40 (7), 755–768.

Cao, C., Love, G.D., Hays, L.E., Wang, W., Shen, S., Summons, R.E., 2009. Biogeochemical evidence for euxinic oceans and ecological disturbance presaging the end-Permian mass extinction event. Earth Planet. Sci. Lett. 281 (3–4), 188–201.

Cribb, A.T., Formoso, K.K., Woolley, C.H., Beech, J., Brophy, S., Byrne, P., Cassady, V.C., Godbold, A.L., Larina, E., Maxeiner, P.P., Wu, Y.H., 2023. Contrasting terrestrial and marine ecospace dynamics after the end-Triassic mass extinction event. Proc. R. Soc. B 290 (2012), 20232232.

Dal Corso, J., Song, H., Callegaro, S., Chu, D., Sun, Y., Hilton, J., Grasby, S.E., Joachimski, M.M., Wignall, P.B., 2022. Environmental crises at the Permian–Triassic mass extinction. Nat. Rev. Earth & Environ. 3 (3), 197–214.

Du, Y., Song, H., Grasby, S.E., Xing, T., Song, H., Tian, L., Chu, D., Wu, Y., Dal Corso, J., Algeo, T.J., Tong, J., 2023. Recovery from persistent nutrient-N limitation following the Permian–Triassic mass extinction. Earth Planet. Sci. Lett. 602, 117944.

Erwin, D.H., Bowring, S.A., Yugan, J., Koeberl, C., MacLeod, K.G., 2002. End-Permian mass extinctions: a review. In: Special Papers-Geological Society of America, pp. 363–384.

Foster, W.J., Lehrmann, D.J., Yu, M., Ji, L., Martindale, R.C., 2018. Persistent environmental stress delayed the recovery of marine communities in the aftermath of the latest Permian mass extinction. Paleoceanogr. Paleoclimatol. 33 (4), 338–353.

Fujisaki, W., Matsui, Y., Ueda, H., Sawaki, Y., Suzuki, K., Maruoka, T., 2022. Pre-treatment methods for accurate determination of total nitrogen and organic carbon contents and their stable isotopic compositions: Re-evaluation from geological reference materials. Geostand. Geoanal. Res. 46, 5–19.

Godbold, A., Schoepfer, S., Shen, S., Henderson, C.M., 2017. Precarious ephemeral refugia during the earliest Triassic. Geology 45 (7), 607–610.

Grasby, S.E., Beauchamp, B., Knies, J., 2016. Early Triassic productivity crises delayed recovery from world's worst mass extinction. Geology 44 (9), 779–782.

Grasby, S.E., Knies, J., Beauchamp, B., Bond, D.P., Wignall, P., Sun, Y., 2020. Global warming leads to early Triassic nutrient stress across northern Pangea. Bulletin 132 (5–6), 943–954.

Grasby, S.E., Bond, D.P.G., Wignall, P.B., Yin, R., Strachan, L.J., Takahashi, S., 2021. Transient Permian-Triassic euxinia in the southern Panthalassa deep ocean. Geology 49 (8), 889–893.

Grice, K., Cao, C., Love, G.D., Böttcher, M.E., Twitchett, R.J., Grosjean, E., Summons, R. E., Turgeon, S.C., Dunning, W., Jin, Y., 2005. Photic zone euxinia during the Permian-Triassic superanoxic event. Science 307 (5710), 706–709.

Hays, L.E., Beatty, T., Henderson, C.M., Love, G.D., Summons, R.E., 2007. Evidence for photic zone euxinia through the end-Permian mass extinction in the Panthalassic Ocean (Peace River Basin, Western Canada). Palaeoworld 16 (1–3), 39–50.

Henderson, C.M., Shen, S.Z., Gradstein, F.M., Agterberg, F.P., 2020. The Permian Period. In: Geologic Time Scale 2020. Elsevier, pp. 875–902.

Isozaki, Y., 1997. Permo-Triassic boundary superanoxia and stratified superocean: records from lost deep sea. Science 276 (5310), 235–238.

Jin, Y.G., Wang, Y., Wang, W., Shang, Q.H., Cao, C.Q., Erwin, D.H., 2000. Pattern of marine mass extinction near the Permian-Triassic boundary in South China. Science 289 (5478), 432–436.

Joachimski, M.M., Lai, X., Shen, S., Jiang, H., Luo, G., Chen, B., Chen, J., Sun, Y., 2012. Climate warming in the latest Permian and the Permian–Triassic mass extinction. Geology 40 (3), 195–198.

Kidder, D.L., Worsley, T.R., 2010. Phanerozoic large igneous provinces (LIPs), HEATT (haline euxinic acidic thermal transgression) episodes, and mass extinctions. Palaeogeogr. Palaeoclimatol. Palaeoecol. 295 (1–2), 162–191.

King, P., Kennedy, H., Newton, P.P., Jickells, T.D., Brand, T., Calvert, S., Cauwet, G., Etcheber, H., Head, B., Khripounoff, A., Manighetti, B., Miquel, J.C., 1998. Analysis of total and organic carbon and total nitrogen in settling oceanic particles and a marine sediment: an interlaboratory comparison. Mar. Chem. 60, 203–216.

Knies, J., Grasby, S.E., Beauchamp, B., Schubert, C.J., 2013. Water mass denitrification during the latest Permian extinction in the Sverdrup Basin, Arctic Canada. Geology 41 (2), 167–170.

Komada, T., Anderson, M.R., Dorfmeier, C.L., 2008. Carbonate removal from costal sediments for the determination of organic carbon and its isotopic signature, δ13C and Δ14C: comparison of fumigation and direct acidification by hydrochloric acid. Limnol. Oceanogr. 6, 254–262.

Korte, C., Kozur, H.W., 2010. Carbon-isotope stratigraphy across the Permian–Triassic boundary: a review. J. Asian Earth Sci. 39 (4), 215–235.

Kump, L.R., Junium, C., Arthur, M.A., Brasier, A., Fallick, A., Melezhik, V., Lepland, A., CČrne, A.E., Luo, G., 2011. Isotopic evidence for massive oxidation of organic matter following the great oxidation event. Science 334 (6063), 1694–1696.

Lau, K.V., Maher, K., Altiner, D., Kelley, B.M., Kump, L.R., Lehrmann, D.J., Silva-Tamayo, J.C., Weaver, K.L., Yu, M., Payne, J.L., 2016. Marine anoxia and delayed Earth system recovery after the end-Permian extinction. Proc. Natl. Acad. Sci. 113 (9), 2360–2365.

Lehrmann, D.J., Payne, J.L., Felix, S.V., Dillett, P.M., Wang, H., Yu, Y., Wei, J., 2003. Permian–Triassic boundary sections from shallow-marine carbonate platforms of the Nanpanjiang Basin, South China: implications for oceanic conditions associated with the end-Permian extinction and its aftermath. Palaios 18 (2), 138–152.

Lehrmann, D.J., Enos, P., Payne, J.L., Montgomery, P., Wei, J., Yu, Y., Xiao, J., Orchard, M.J., 2005. Permian and Triassic depositional history of the Yangtze platform and Great Bank of Guizhou in the Nanpanjiang basin of Guizhou and Guangxi, South China. Albertiana 33 (1), 149–168.

Li, Z., Jia, G., 2011. Separation of total nitrogen from sediments into organic and inorganic forms for isotopic analysis. Org. Geochem. 42 (3), 296–299.

Lucas, S.G., Shen, S.Z., 2018. The Permian Timescale: An Introduction, 450, No. 1. The Geological Society of London, London, pp. 1–19.

Luo, G., Wang, Y., Algeo, T.J., Kump, L.R., Bai, X., Yang, H., Yao, L., Xie, S., 2011. Enhanced nitrogen fixation in the immediate aftermath of the latest Permian marine mass extinction. Geology 39 (7), 647–650.

Meyers, P.A., 1994. Preservation of elemental and isotopic source identification of sedimentary organic matter. Chem. Geol. 114 (3–4), 289–302.

Payne, J.L., Lehrmann, D.J., Follett, D., Seibel, M., Kump, L.R., Riccardi, A., Altiner, D., Sano, H., Wei, J., 2007. Erosional truncation of uppermost Permian shallow-marine carbonates and implications for Permian-Triassic boundary events. Geol. Soc. Am. Bull. 119 (7–8), 771–784.

Payne, J.L., Turchyn, A.V., Paytan, A., DePaolo, D.J., Lehrmann, D.J., Yu, M., Wei, J., 2010. Calcium isotope constraints on the end-Permian mass extinction. Proc. Natl. Acad. Sci. 107 (19), 8543–8548.

Penn, J.L., Deutsch, C., Payne, J.L., Sperling, E.A., 2018. Temperature-dependent hypoxia explains biogeography and severity of end-Permian marine mass extinction. Science 362 (6419) p.eaat1327.

Pietsch, C., Ritterbush, K.A., Thompson, J.R., Petsios, E., Bottjer, D.J., 2019. Evolutionary models in the early Triassic marine realm. Palaeogeogr. Palaeoclimatol. Palaeoecol. 513, 65–85.
Riccardi, A.L., Arthur, M.A., Kump, L.R., 2006. Sulfur isotopic evidence for chemocline upward excursions during the end-Permian mass extinction. Geochim. Cosmochim. Acta 70 (23), 5740–5752.
Romano, C., Goudemand, N., Vennemann, T.W., Ware, D., Schneebeli-Hermann, E., Hochuli, P.A., Brühwiler, T., Brinkmann, W., Bucher, H., 2013. Climatic and biotic upheavals following the end-Permian mass extinction. Nat. Geosci. 6 (1), 57–60.
Schobben, M., Stebbins, A., Ghaderi, A., Strauss, H., Korn, D., Korte, C., 2015. Flourishing Ocean drives the end-Permian marine mass extinction. Proc. Natl. Acad. Sci. 112 (33), 10298–10303.
Schoepfer, S.D., 2014. Nutrients, Productivity, and Redox Conditions during Greenhouse Extinctions in the Panthalassic Ocean (Doctoral Dissertation).
Schoepfer, S.D., Henderson, C.M., 2021. Paleogeographic implications of open-marine anoxia in the Permian–Triassic slide mountain ocean. Late Paleozoic and Early Mesozoic Tectonostratigraphy and Biostratigraphy of Western Pangea, SEPM Special Publication 113. Soc. Sediment. Geol. 2022, 205–225.
Schoepfer, S.D., Henderson, C.M., Garrison, G.H., Ward, P.D., 2012. Cessation of a productive coastal upwelling system in the Panthalassic Ocean at the Permian–Triassic boundary. Palaeogeogr. Palaeoclimatol. Palaeoecol. 313, 181–188.
Schoepfer, S.D., Henderson, C.M., Garrison, G.H., Foriel, J., Ward, P.D., Selby, D., Hower, J.C., Algeo, T.J., Shen, Y., 2013. Termination of a continent-margin upwelling system at the Permian–Triassic boundary (Opal Creek, Alberta, Canada). Glob. Planet. Chang. 105, 21–35.
Shen, S.Z., Wang, Y., Henderson, C.M., Cao, C.Q., Wang, W., 2007. Biostratigraphy and lithofacies of the Permian System in the Laibin–Heshan area of Guangxi, South China. Palaeoworld 16 (1–3), 120–139.
Shen, J., Schoepfer, S.D., Feng, Q., Zhou, L., Yu, J., Song, H., Wei, H., Algeo, T.J., 2015. Marine productivity changes during the end-Permian crisis and early Triassic recovery. Earth Sci. Rev. 149, 136–162.
Shen, S.Z., Ramezani, J., Chen, J., Cao, C.Q., Erwin, D.H., Zhang, H., Xiang, L., Schoepfer, S.D., Henderson, C.M., Zheng, Q.F., Bowring, S.A., 2019. A sudden end-Permian mass extinction in South China. GSA Bull. 131 (1–2), 205–223.
Sigman, D.M., Altabet, M.A., McCorkle, D.C., Francois, R., Fischer, G., 2000. The δ15N of nitrate in the Southern Ocean: Nitrogen cycling and circulation in the ocean interior. J. Geophys. Res. Oceans 105 (C8), 19599–19614.
Song, H., Tong, J., Xiong, Y., Sun, D., Tian, L., Song, H., 2012. The large increase of δ13C carb-depth gradient and the end-Permian mass extinction. Sci. China Earth Sci. 55, 1101–1109.
Song, H., Wignall, P.B., Chu, D., Tong, J., Sun, Y., Song, H., He, W., Tian, L., 2014. Anoxia/high temperature double whammy during the Permian-Triassic marine crisis and its aftermath. Sci. Rep. 4 (1), 4132.
Stüeken, E., Pellerin, A., Thomazo, C., Johnson, B., Duncanson, S., Schoepfer, S., 2024. Marine Biogeochemical Nitrogen Cycling through Earth's History. Nature Reviews Earth & Environment. Accepted, (in press).
Sun, Y., Joachimski, M.M., Wignall, P.B., Yan, C., Chen, Y., Jiang, H., Wang, L., Lai, X., 2012. Lethally hot temperatures during the early Triassic greenhouse. Science 338 (6105), 366–370.
Sun, Y.D., Zulla, M.J., Joachimski, M.M., Bond, D.P.G., Wignall, P.B., Zhang, Z.T., Zhang, M.H., 2019. Ammonium ocean following the end-Permian mass extinction. Earth Planet. Sci. Lett. 518, 211–222.
Wignall, P.B., Twitchett, R.J., 2002. Extent, duration, and nature of the Permian-Triassic superanoxic event. In: Catastrophic Events and Mass Extinctions: Impacts and beyond. Geological Society of America, pp. 395–413.
Xiang, L., Zhang, H., Schoepfer, S.D., Cao, C.Q., Zheng, Q.F., Yuan, D.X., Cai, Y.F., Shen, S.Z., 2020. Oceanic redox evolution around the end-Permian mass extinction at Meishan, South China. Palaeogeogr. Palaeoclimatol. Palaeoecol. 544, 109626.
Xiang, L., Schoepfer, S.D., Yuan, D.X., Zheng, Q.F., Zhang, H., 2022. Oceanic redox evolution across the end-Permian mass extinction at Penglaitan section, South China. Palaeoworld 31 (1), 93–102.
Yin, H., Feng, Q., Lai, X., Baud, A., Tong, J., 2007. The protracted Permo-Triassic crisis and multi-episode extinction around the Permian–Triassic boundary. Glob. Planet. Chang. 55 (1–3), 1–20.
Yin, H., Jiang, H., Xia, W., Feng, Q., Zhang, N., Shen, J., 2014. The end-Permian regression in South China and its implication on mass extinction. Earth Sci. Rev. 137, 19–33.
Yuan, D.X., Shen, S.Z., Henderson, C.M., Chen, J., Zhang, H., Feng, H.Z., 2014. Revised conodont-based integrated high-resolution timescale for the Changhsingian Stage and end-Permian extinction interval at the Meishan sections, South China. Lithos 204, 220–245.
Zakharov, Y.D., Horacek, M., Biakov, A.S., 2021. Variations in Nitrogen Isotope Composition in Clay Deposits of the Permian–Triassic Boundary Beds in the Verkhoyansk Region (Northeast Asia) and Their Implication for Reconstruction of Marine Environments. Stratigr. Geol. Correl. 29, 192–214.
Zhang, X., McRose, D.L., Darnajoux, R., Bellenger, J.P., Morel, F.M., Kraepiel, A.M., 2016. Alternative nitrogenase activity in the environment and nitrogen cycle implications. Biogeochemistry 127, 189–198.
Zhang, F., Algeo, T.J., Romaniello, S.J., Cui, Y., Zhao, L., Chen, Z.Q., Anbar, A.D., 2018a. Congruent Permian-Triassic δ238U records at Panthalassic and Tethyan sites: Confirmation of global-oceanic anoxia and validation of the U-isotope paleoredox proxy. Geology 46 (4), 327–330.
Zhang, Y., Wen, H., Zhu, C., Fan, H., Cloquet, C., 2018b. Cadmium isotopic evidence for the evolution of marine primary productivity and the biological extinction event during the Permian-Triassic crisis from the Meishan section, South China. Chem. Geol. 481, 110–118.
Zhong, Y.T., He, B., Xu, Y.G., 2013. Mineralogy and geochemistry of claystones from the Guadalupian–Lopingian boundary at Penglaitan, South China: insights into the pre-Lopingian geological events. J. Asian Earth Sci. 62, 438–462.